Biomaterials 35 (2014) 9897–9903

Contents lists available at ScienceDirect

Biomaterials

journal homepage: www.elsevier.com/locate/biomaterials

The control of cargo release from physically crosslinked hydrogels by crosslink dynamics

Eric A. Appel, Rebecca A. Forster, Matthew J. Rowland, Oren A. Scherman*

Melville Laboratory for Polymer Synthesis, Department of Chemistry, Cambridge University, Lensfield Road, Cambridge CB2 1EW, UK

ARTICLE INFO

Article history:
Received 16 June 2014
Accepted 1 August 2014
Available online 16 September 2014

Keywords:
Drug delivery
Drug release
Hydrogel
Mechanical properties
Cross-linking
Controlled drug release

ABSTRACT

Controlled release of drugs and other cargo from hydrogels has been an important target for the development of next generation therapies. Despite the increasingly strong focus in this area of research, very little of the published literature has sought to develop a fundamental understanding of the role of molecular parameters in determining the mechanism and rate of cargo release. Herein, a series of physically crosslinked hydrogels have been prepared utilizing host-guest binding interactions of cucurbit [8]uril that are identical in strength (plateau modulus), concentration and structure, yet exhibit varying network dynamics on account of the use of different guests for supramolecular crosslinking. The diffusion of molecular cargo through the hydrogel matrix and the release characteristics from these hydrogels were investigated. It was determined that the release processes of the hydrogels could be directly correlated with the dynamics of the physical interactions responsible for crosslinking and corresponding time-dependent mesh size. These observations highlight that network dynamics play an indispensable role in determining the release mechanism of therapeutic cargo from a hydrogel, identifying that fine-tuning of the release characteristics can be gained through rational design of the molecular processes responsible for crosslinking in the carrier hydrogels.

1. Introduction

Hydrogels are an important class of biomaterial that have received much attention for controlled drug-delivery applications on account of their similarity to soft biological tissue and highly variable mechanical properties [1–6]. Modeling of the controlled release of drugs and other cargo from these polymeric devices has been a subject of considerable research and many reviews have been published to address the principles of modelling diffusional release [7–9]. Many models in the past have focused on Fickian diffusion [10] however, Peppas and coworkers [11–13], have derived an important and exceedingly simple exponential relationship to describe the general release behavior of cargo from a controlled release polymeric device:

$$\frac{M_t}{M_\infty} = kt^n \quad (1)$$

The equation relates both a release constant (k) and a diffusional exponent (n), which is characteristic of the release mechanism. While pure Fickian diffusion from such a polymeric device yields an n value of 0.50, values above this limit occur in systems that display some amount of anomalous release. Indeed, greater deviation from $n = 0.50$ signifies a greater contribution of anomalous release to the overall release mechanism. This equation has been applied in a wide variety of instances to describe drug-delivery phenomena including pH-swellable devices [14] and highly swellable polymers [15].

Although the work by Peppas et al. focused primarily on chemically crosslinked hydrogels, the simple mathematical relationship has been utilized in describing delivery of cargo from a wide variety of physically crosslinked hydrogels [4,16–18]. Physical crosslinking arises from entanglements between macromolecular species where specific and dynamic non-covalent interactions are used as the structural crosslinks between polymer chains, thereby coupling many of the exceptional qualities of polymer-based hydrogels with the diversity and orthogonality of supramolecular chemistry [19–22]. These hydrogels are particularly interesting on account of their dynamic nature, which can be regarded as an advantageous characteristic as it is the basis for both shear-thinning (viscous flow under shear stress) and self-healing (recovery after network damage) properties, two desirable characteristics for a variety of important applications [6,23,24]. These types of materials

* Corresponding author. Fax: +44 (0)1223 334866.
E-mail address: oas23@cam.ac.uk (O.A. Scherman).

http://dx.doi.org/10.1016/j.biomaterials.2014.08.001
0142-9612/

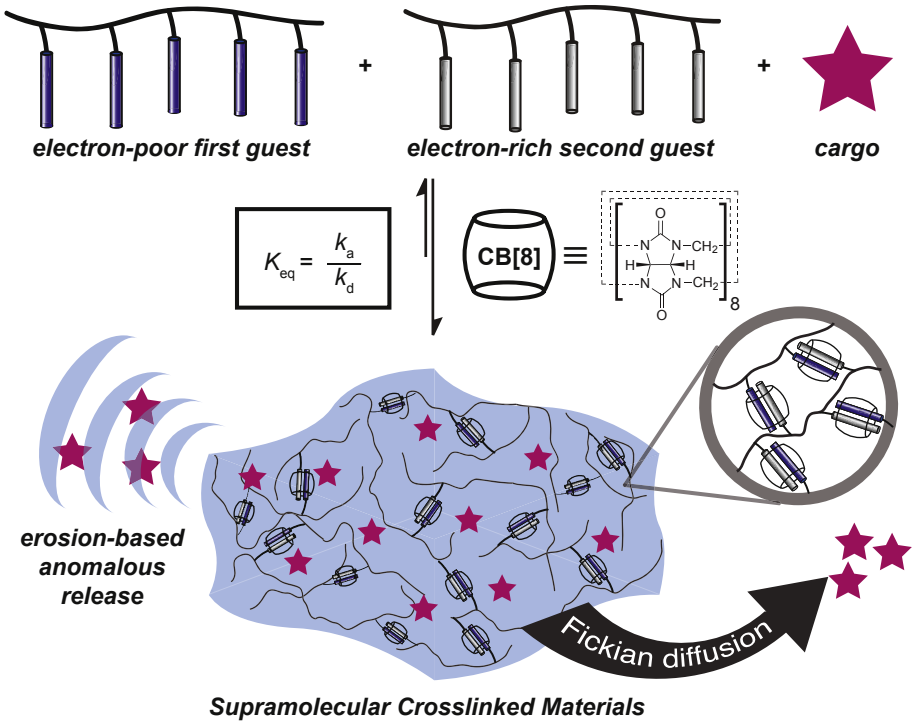

Fig. 1. Schematic representation of the preparation of dynamically crosslinked hydrogels utilizing cucurbit[8]uril host-guest chemistry. Physical crosslink dynamics, arising from the CB[8] ternary complex, play an important role in determining the release mechanism (a combination of erosion-based and Fickian diffusional release) of a model drug from the materials.

have displayed exceptional utility within the field of biomedicine, in part on account of the fact that they do not require surgical procedures since they can be pre-formed *ex vivo* and then delivered in a minimally invasive manner *in vivo* by applying shear stress when injected through a syringe. This method for implantation has been demonstrated to provide a more uniform distribution of cells or other therapeutic cargo in the injected gel [25] and greater control over placement of the material *in vivo* [26].

The release characteristics of cargo from these physically crosslinked materials, however, is conceivably more complex than chemically crosslinked materials on account of their ability to erode from the surface, thereby giving rise to a different mechanism for anomalous release from the device. In these systems, therefore, the diffusional exponent (n) can be utilized to characterize the contribution of erosion to the overall release profile of the cargo. Moreover, it is well known that the physical characteristics of such hydrogels, including their erosion behavior and rheology, arise from a combination of two fundamental characteristics: (a) supramolecular interactions responsible for the dynamic crosslinking and (b) conventional polymer physics describing polymer interactions within the material [2,3]. Elucidation of the role of the fundamental parameters of supramolecular crosslinking in determining the macroscopic behavior of these materials has only recently been achieved [27–29]. As an enormous array of supramolecular units have been utilized in the preparation of physically crosslinked materials over the past two decades, the ability to discern their specific role in determining the controlled release behavior from these polymeric devices is paramount for designing the next generation of such systems.

Our laboratory has previously demonstrated the preparation of physically crosslinked hydrogels based on the strong and highly specific hetero-ternary complex formation of the macrocyclic host cucurbit[8]uril (CB[8]) [30–33]. Cucurbit[n]uril ($n = 5$–8, 10; CB[n]) are a family of macrocyclic host molecules that are oligomers of glycoluril, which exhibit a symmetric 'barrel' shape with two identical portal regions laced by ureido-carbonyl oxygens. The number of glycoluril units determines the size of the cucurbituril cavity without affecting the height of the molecular container (approximately 0.9 nm), similar to the cyclodextrin (CD) family. While smaller homologs of the CB[n] family (*i.e.* CB[5], CB[6] and CB[7]) are capable of binding single guests (typically cationic amines, metal or imidazolium ions) [34–37], CB[8] has a larger cavity volume and can simultaneously accommodate two guests (Fig. 1) [38]. An electron-deficient first guest, such as methyl viologen (MV), and an electron-rich second guest, typically flat aromatic compounds such as naphthyl derivatives, form a stable 1:1:1 ternary complex with CB[8] through multiple non-covalent interactions acting synergistically, resulting in exceptionally high equilibrium binding affinities (K_{eq} up to 10^{14} M^{-2}) [39]. This motif has been utilized previously in the preparation of supramolecular polymeric hydrogels [30–33] and other crosslinked polymeric materials [40] using naphthalene derivatives as the electron-rich second guest. Recently, we have developed a series of ternary complexes whereby the binding of the second-guest moieties display a range of associative and dissociative rate constants (k_a and k_d, respectively) and activation energies for the associative and dissociative processes (Ea_a and Ea_d, respectively) while exhibiting identical thermodynamic equilibrium constants (K_{eq}) [29]. Utilizing these guests for the preparation of physically crosslinked hydrogels has given rise to a series of materials with identical plateau storage moduli (G′; on account their identical K_{eq} values) and structure, yet exhibiting varying network dynamics on account of the different molecular kinetics governing supramolecular crosslinking [29]. The varying dynamics of the second-guest binding, therefore, yield physical crosslinks with varying lifetimes arising from the differences in the energy required to convert an 'active' (bound) crosslink to and 'inactive' (un-bound) species.

Herein, we report the encapsulation and *in vitro* release of Rhodamine-B by these hydrogels (Fig. 1). Rhodamine-B is a

common water-soluble imaging agent used in microscopy, flow cytometry and ELISA, among others, and is used here as a simple model cargo. These studies are aimed at discovering the effect of the molecular dynamics of the physical crosslinking of hydrogels on the release characteristics of molecular cargo.

2. Experimental methods

2.1. Materials and methods

^{1}H NMR (400 MHz) spectra were recorded using a Bruker Avance QNP 400. Chemical shifts are recorded in ppm (δ) in $CDCl_3$ with the internal reference set to $\delta = 7.26$ ppm .^{13}C NMR (125 MHz) spectra were recorded using a Bruker Avance QNP 400. Chemical shifts are recorded in ppm (δ) in $CDCl_3$ with the internal reference set to $\delta = 77.16$ ppm. ATR FT-IR spectroscopy was performed using a Perkin–Elmer Spectrum 100 series FT-IR spectrometer equipped with a universal ATR sampling accessory. UV-VIS studies were performed on a Varian Cary 4000 UV-Vis spectrophotometer. Gel permeation chromatography (GPC) was carried out in tetrahydrofuran (THF) on two Jordi divinylbenzene columns connected in series with a Shimadzu SPD-M20A prominence photodiode array detector, Optilab refractive index detector and MALLS detector (both Wyatt). Samples were filtered over 0.2 μm PTFE filters before injection using a 1.0 mL/min flow rate. Molecular weights and polydispersities were determined using analysis of the MALLS and refractive index data using ASTRA software by Wyatt.

Rheological characterization was performed using a TA Instruments DHR2 controlled stress rheometer fitted with a peltier stage set to 37 °C. Dynamic oscillatory strain amplitude sweep measurements were conducted at a frequency of 10 rad/s. Dynamic oscillatory frequency sweep measurements were conducted at a 10% strain amplitude. All measurements were performed using a 40 mm parallel plate geometry with a gap of 0.500 mm and analyzed using TA Instruments TRIOS software.

Poly(StMV-*r*-StAm) [30], cucurbit[8]uril [38], and 2-((((2-carboxyethyl)thio) carbonothioyl)thio)-2-methylpropanoic acid (CECMP) [41] were prepared according to literature procedures. All other materials were purchased from Aldrich and used as received.

2.2. Synthesis of functional polymers

2.2.1. Synthesis of 2-isocyanato-3-methoxydibenzo[b,d]furan (DBF-NCO)

A stirred solution of 2-amino-3-methoxydibenzo[b,d]furan (3.6 g, 17 mmol) and triethylamine (3.2 mL, 25 mmol) in 150 mL anhydrous DCM was cooled in an ice-bath, and triphosgene (5.5 g, 19 mmol) was added in several portions. The ice-bath was removed after 1 h and the mixture was stirred at room temperature for 24 h. Purification was achieved by flash chromatography on silica with DCM to yield the title compound (3.5 g, 16 mmol, 87%) as an off-white solid. ^{1}H NMR (400 MHz, $CDCl_3$): $\delta = 7.91$ (d, 1H, 7.7 Hz), 7.58 (d, 1H, 8.3 Hz), 7.50–7.45 (m, 1H), 7.40–7.36 (m, 2H), 7.25 (s, 1H), 4.08 (s, 3H) ppm. ^{13}C NMR (125 MHz, $CDCl_3$): $\delta = 156.8, 150.2, 130.8, 126.8, 124.2, 123.6, 122.7, 121.3, 120.1, 111.7, 107.1, 101.5, 56.51$ ppm. FT-IR: $\bar{\nu} = 2228$ cm^{-1} (–NCO).

2.2.2. Synthesis of 1-pyrene isocyanate (Pyr-NCO)

1-Pyrene isocyanate was synthesized from 1-pyrene amine in analogy to the above described procedure for DBF-NCO to yield the title compound (1.2 g, 5 mmol, 80%) as a pale green solid. ^{1}H NMR (400 MHz, $CDCl_3$): $\delta = 8.20–8.13$ (m, 3H), 8.06–7.93 (m, 5H), 7.70 (d, 1H, 8.1 Hz) ppm. ^{13}C NMR (125 MHz, $CDCl_3$): $\delta = 129.3, 129.1, 127.2, 126.4, 125.4, 125.0, 124.8, 124.5, 123.6, 123.4, 123.3, 123.2, 122.3, 121.2, 119.8$ ppm. FTIR: $\bar{\nu} = 2249$ cm^{-1} (–NCO).

2.2.3. Synthesis of PDMAm-Pyr

PYR-NCO (1.0 g, 4.1 mmol) and *N*-hydroxyethylacrylamide (0.47 g, 4.1 mmol) was dissolved in DCM (15 mL) and 3 drops of triethylamine was added and the mixture stirred at room temperature for 16 h. A precipitate formed and was filtered off to yield pyrene functional acrylamide monomer (PyrAm) as a white solid (1.45 g, 98%) and was used without further purification. PyrAm (0.75 g, 2.1 mmol, target [M]/[I] = 25), *N*,*N*-dimethylacrylamide (3.92 g, 39.5 mmol, target [M]/[I] = 475), CECMP (22.3 mg, 83.1 μmol) and ACPA (4.7 mg, 16.6 μmol) were dissolved in DMSO (20 mL) and the reaction mixture was degassed by bubbling N_2 for 30 min before heating to 70 °C for 12 h. The reaction mixture was then cooled to room temperature in a water bath and the polymer purified by precipitation from cold diethyl ether to yield the title compound as a yellowish amorphous solid (4.5 g, 96%). ^{1}H NMR (400 MHz, $CDCl_3$): δ = 9.17–9.10 (52H, N*H*), 8.30–7.30 (225H, Pyr*H*), 4.55–4.45 (52H, –NHCOO–CH_2–), 4.00–1.30 (4530H, polymer backbone and –CON(CH_3)–), 1.25 (6H, HOOC–C(CH_3)$_2$–) ppm. GPC (THF): M_n (PDI) = 11.0 kDa (1.19).

2.2.4. Synthesis of PDMAm-DBF

DBF-NCO (1.0 g, 4.2 mmol) and *N*-hydroxyethylacrylamide (0.48 g, 4.2 mmol) was dissolved in DCM (15 mL) and 3 drops of triethylamine was added and the mixture stirred at room temperature for 16 h. A precipitate formed and was filtered off to produce dibenzofuran functional acrylamide monomer (DBFAm) as a white solid (1.45 g, 98%) and was used without further purification. DBFAm (0.74 g, 2.1 mmol, target [M]/[I] = 25), *N*,*N*-dimethylacrylamide (3.92 g, 39.5 mmol, target [M]/[I] = 475), CECMP (22.3 mg, 83.1 μmol) and ACPA (4.7 mg, 16.6 μmol) were dissolved in DMSO (20 mL) and the reaction mixture was degassed by bubbling N_2 for 30 min before heating to 70 °C for 12 h. The reaction mixture was then cooled to room temperature in a water bath and the polymer purified by precipitation from cold diethyl ether to yield the title compound as an off-white amorphous solid (4.5 g, 98%). ^{1}H NMR (400 MHz, $CDCl_3$): δ = 9.17–9.10 (52H, N*H*), 8.30–7.30 (153H, DBF*H*), 4.55–4.45 (52H, –NHCOO–CH_2–), 4.00–1.30 (4580H, polymer backbone and DBF-O-CH_3 and –CON(CH_3)–), 1.25 (6H, HOOC–C(CH_3)$_2$–) ppm. GPC (THF): M_n (PDI) = 11.7 kDa (1.19).

2.2.5. Synthesis of PDMAm-Np

NP-NCO (commercially available, 1.0 g, 5.9 mmol) and *N*-hydroxyethylacrylamide (0.68 g, 5.9 mmol) was dissolved in DCM (15 mL) and 3 drops of triethylamine was added and the mixture stirred at room temperature for 16 h. The reaction mixture was then run through a short plug of silica gel and the solvent was removed under vacuum, yielding naphthalene functional acrylamide monomer (NpAm) as a white solid (1.61 g, 96%), which was used without further purification. NpAm (0.59 g, 2.1 mmol, target [M]/[I] = 25), *N*,*N*-dimethylacrylamide (3.92 g, 39.5 mmol, target [M]/[I] = 475), CECMP (22.3 mg, 83.1 μmol) and ACPA (4.7 mg, 16.6 μmol) were dissolved in DMSO (20 mL) and the reaction mixture was degassed by bubbling N_2 for 30 min before heating to 70 °C for 12 h. The reaction mixture was then cooled to room temperature in a water bath and the polymer purified by precipitation from cold diethyl ether to yield the title compound as a white amorphous solid (4.3 g, 95%). ^{1}H NMR (400 MHz, $CDCl_3$): δ = 9.17–9.10 (52H, N*H*), 8.30–7.30 (179H, Np*H*), 4.55–4.45 (52H, –NHCOO–CH_2–), 4.00–1.30 (4500H, polymer backbone and –CON(CH_3)–), 1.25 (6H, HOOC–C(CH_3)$_2$–) ppm. GPC (THF): M_n (PDI) = 12.0 kDa (1.20).

2.3. General preparation of self-assembled hydrogels

Hydrogels were prepared by first dissolving PDMAm-G2 (13 mg) in water (0.5 mL) with stirring. StAm-StMV (15 mg) and CB[8] (10 mg) were then dissolved in water (0.5 mL) with the aid of some sonication (less than 5 min). The solutions were then added together, heated with a heat gun, and mixed vigorously with vortex for approximately 10 s for hydrogel formation.

2.4. Release studies from hydrogels

Hydrogels were prepared as mentioned above using Rhodamine-B dye (0.01 mg/mL) solutions instead of pure water resulting in a final Rhodamine-B dye concentration of 0.01 mg/mL in the hydrogels. In a typical example, 1.0 mL of dye loaded hydrogel was prepared in a sample vial (standard 0.5 dram vials). Water (2.0 mL) was then added on top of the hydrogel. The aqueous solutions were replaced with fresh ones at predetermined time intervals, and the experiments were performed in triplicate. The collected aqueous solutions were analyzed for dye concentration based on a calibration curve prepared using Rhodamine-B absorbance at 554 nm. The samples were then lyophilized and analyzed for polymer concentration.

3. Results and discussion

3.1. Functional polymeric building blocks

Radical polymerization techniques were utilized in the preparation of multivalent side-chain functional polymer building blocks bearing either viologen (MV) or second guest (G2) derivatives. A styrenic monomer bearing an MV moiety (StMV) was readily synthesized on a large scale from 4-vinylbenzylchloride and methyl bipyridine in high yields (>85%). (Vinylbenzyl)trimethylammonium chloride (StAm) was chosen as a styrenic comonomer in order to ensure a random distribution of the guest moieties along the polymer chains. An MV-functional copolymer was then synthesized by traditional 'uncontrolled' free radical polymerization following a method reported in the literature (Fig. 2b) [30]. This copolymer (StAm-*r*-StMV) was prepared with 5% molar loading of functional styrenic StMV according to ^{1}H NMR spectroscopic characterization.

For the preparation of second-guest functional copolymers, pyrenyl (PYR), dibenzofuranyl (DBF), and naphthyl (NP) guests were functionalized with isocyanates [42] and conjugated to *N*-hydroxyethylacrylamide monomers. These guests were chosen as they display a range of associative and dissociative rate constants ($k_a$and k_d, respectively) and corresponding activation energies of association and dissociation ($Ea_a$and Ea_d, respectively) while

exhibiting identical thermodynamic equilibrium constants (K_{eq}) [29]. These guest functional acrylamide monomers (G2Am) allowed for facile copolymerization with *N*,*N*-dimethylacrylamide comonomers yielding non-ionic, water-soluble polymers. Reversible addition-fragmentation chain transfer (RAFT) polymerization was used for the preparation of several multivalent, second-guest functional copolymers with a well known trithiocarbonate-based chain transfer agent (CTA) 2-((((2-carboxyethyl)thio)carbonothioyl)thio)-2-methylpropanoic acid (CECMP) [41] using standard RAFT conditions in DMSO (Fig. 2a). CECMP was used as it successfully mediates the polymerization of a wide variety of monomers (styrenics, (meth)acrylates, and (meth)acrylamides) in a variety of solvent conditions with high control over molecular weight and yielding low polydispersities (PDI) [41]. A series of copolymers of equivalent molecular weight and polydispersity were prepared bearing 5% loading of the second-guest functional monomers (PDMAm-G2; Table 1). ^{1}H NMR analysis verified that the targeted loading of functional monomer and overall molecular weight was achieved by comparing resonances arising from the aryl moieties of the guests, the methyl groups from the DMA comonomer, and from the methylene in the α-position relative to the trithiocarbonate end-group retained in the final polymers. GPC analysis of these polymers demonstrated that an exact overlay existed with both refractive index and UV-vis detectors, demonstrating that each polymer bears both second-guest moieties and the trithiocarbonate from the RAFT CTA.

Table 1
Preparation of second guest functional PDMAm-G2 polymers used in this study.

Guest	$Guest_{theo}$ (%)	$Guest_{exp}$ (%)[a]	M_n (kDa)[a]	M_n (kDa)[b]	PDI[b]
NP	5.0	5.0	52.2	12.0	1.20
DBF	5.0	5.0	53.1	11.7	1.19
PYR	5.0	5.0	54.5	11.0	1.19

[a] Determined by ^{1}H NMR.
[b] Determined by H_2O GPC.

3.2. Dynamically crosslinked hydrogels

These various guests have been utilized to prepare a series of physically crosslinked materials exhibiting identical plateau storage moduli (G′; on account their identical K_{eq} values), yet varying network dynamics arising from differences in the molecular kinetics governing formation of the ternary complex (*vide infra*). Hydrogels were prepared by simply mixing aqueous solutions of the first guest functional polymer P(StAm-StMV) and a second guest functional polymer P(DMAm-G2) in the presence of CB[8]. A series of hydrogels containing identical polymer loading were prepared, differing only in the second guest used, and therefore the fundamental parameters governing crosslinking. Oscillatory rheological characterization of these materials was performed at 37 °C and is demonstrated in Fig. 3a. It has previously been determined that the viscoelasticity of these physically crosslinked materials arises exclusively from the energetic barrier to dissociation (Ea_d) and that materials formed with pyrenyl derivatives, those exhibiting the highest Ea_d values (Ea_d = 89 kJ/mol) in the series prepared, demonstrate the lowest crossover frequency of the storage and loss modulus (G′ and G″, respectively) [29]. Likewise, dibenzofuranyl derivatives exhibit intermediate behavior on account of their intermediate energetic barrier values (Ea_d = 54 kJ/mol), while naphthyl derivatives exhibit the lowest energetic barrier to dissociation (Ea_d = 30 kJ/mol) and a correspondingly high G′/G″ crossover frequency. Hydrogels with a lower barrier to the dissociation of a physical crosslink, therefore, exhibit more fluid-like behavior. Moreover, Fig. 3b demonstrates the exact overlay of the rheological data that occurs upon normalization with the respective Ea_d values of the ternary complexes used in each material, indicating that the bulk mechanical properties of the materials are indeed scalable with molecular parameters.

3.3. Release characteristics from dynamically crosslinked hydrogels

Similar to previous reports of drug loaded CB[8]-based hydrogels [32], Rhodamine-B (our model cargo) was easily incorporated into these hydrogels (Fig. 1) by mixing the dye into the aqueous polymer solutions before hydrogel formation. The release profiles for the model cargo from the hydrogels are demonstrated in Fig. 4a. Release of the cargo occurs more rapidly from hydrogels prepared utilizing guests with faster dissociation kinetics and lower activation energies of dissociation. In order to further probe this behavior, the release profile from each of the polymeric materials was fitted to the Ritger–Peppas equation for drug release [11–13], as shown in Fig. 4b. It is

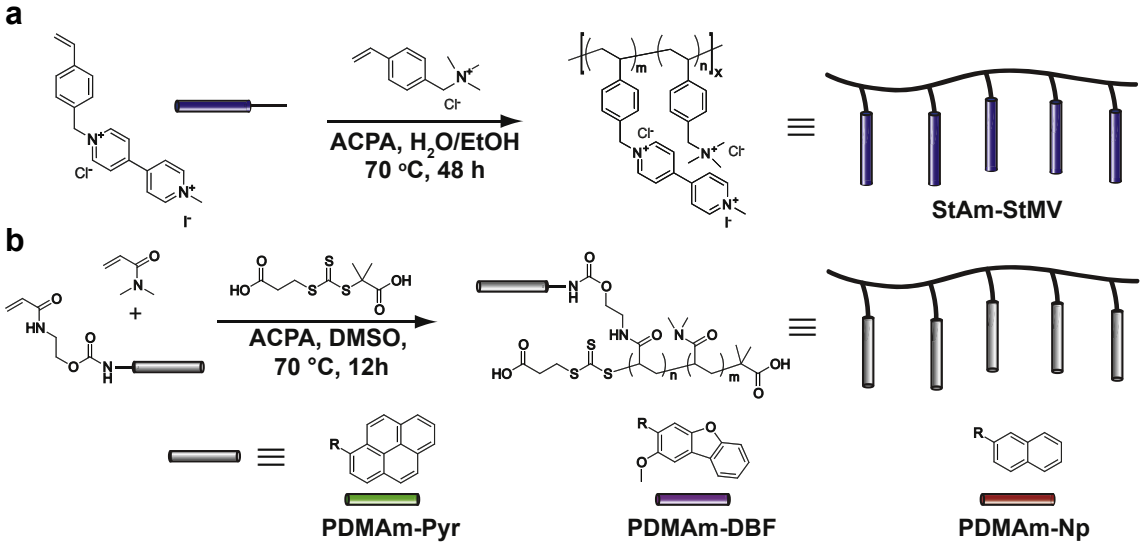

Fig. 2. Schematic representation of the synthesis of a. first guest functional polymers (StAm-StMV) by traditional free radical polymerization reported previously [30] and b. second guest functional dimethylacrylamide polymers (PDMAm-G2) by RAFT polymerization.

evident from Fig. 4b that the rate constant $k_{release}$ of the release profile is hydrogel dependent, and therefore dependent on the crosslink dynamics, while the diffusional coefficient n is not. Pure Fickian diffusional release, as mentioned previously, is described by a diffusional coefficient of $n = 0.5$, with $n > 0.5$ revealing a greater contribution of erosion to the overall release profile. These materials, therefore, exhibit almost pure Fickian diffusional release, and the insensitivity of the diffusional coefficient to crosslink dynamics in this particular series is likely on account of the high diffusional release rates relative to the rate of erosion of the hydrogels (*vide infra*).

Higher release constants ($k_{release}$) are observed for the samples with *smaller* Ea_d values and *faster* crosslink kinetics, highlighting that more rapid crosslink dynamics allow for faster diffusional release (Table 2 and Fig. 5a). These observations can be understood by considering that when the energetic barrier to crosslink dissociation is higher (*i.e.* when PYR is used as a crosslinking moiety), the lifetime of the crosslinks is longer and therefore diffusion of the solute through the polymeric material is slower. This phenomena is likely on account of the fact that the small polymeric mesh structure of these materials (approximately 10 Å) [29] is more static and therefore the 'gates' (*i.e.* the polymer mesh) can be seen as being 'closed' to cargo diffusion and release. Alternatively, when a smaller barrier to physical crosslink dissociation exists, as in the case of NP, the cargo is permitted to diffuse more rapidly through the network on account of the 'gates' being 'open' more often.

Diffusion rates can be determined from the fractional release at short timescales (up to 60% released) with the highly useful approximation shown below,

$$\frac{M_t}{M_\infty} = \left[1 - \exp\left(-k(Dt/L)^a\right)\right]^{\frac{1}{b}} \quad (2)$$

where k, a, and b are empirically determined constants that are geometry specific [43]. Diffusion coefficients (D) are plotted against the dissociative activation energy of the dynamic crosslinks in Fig. 5b. An *upper* limit of the diffusion coefficient of the model drug in this polymeric system can be estimated using the Stokes-Einstein equation from the hypothetical case where there is no crosslinking between the polymer chains (*i.e.* the solute is diffusing through a polymer solution and $Ea_d \rightarrow 0$). According to the Stokes-Einstein equation,

$$D = \frac{k_B T}{6\pi\eta r} \quad (3)$$

where k_B is Boltzmann's constant, T is the absolute temperature, η is the solution viscosity, and r is the solute radius of gyration (R_g = 7.8 Å) [44]. Moreover, a *lower* limit of the solute diffusion coefficient can be estimated according to standard theories

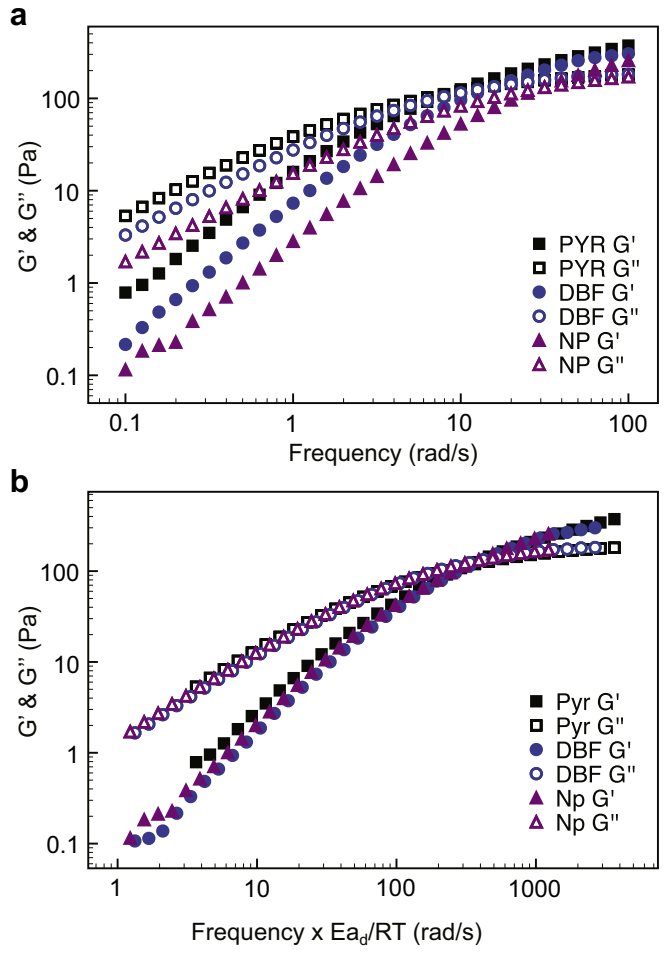

Fig. 3. a. Rheological characterization performed at 37 °C of hydrogels prepared with varying physical crosslinking dynamics by employing different second guest functional polymers (PDMAm-G2) for CB[8] complex formation. b. Scaling of the rheological data with the unit-less activation energies of dissociation $\left(\frac{Ea_d}{RT}\right)$ for each of the second guests participating in crosslinking, clearly demonstrating overlay of the data sets.

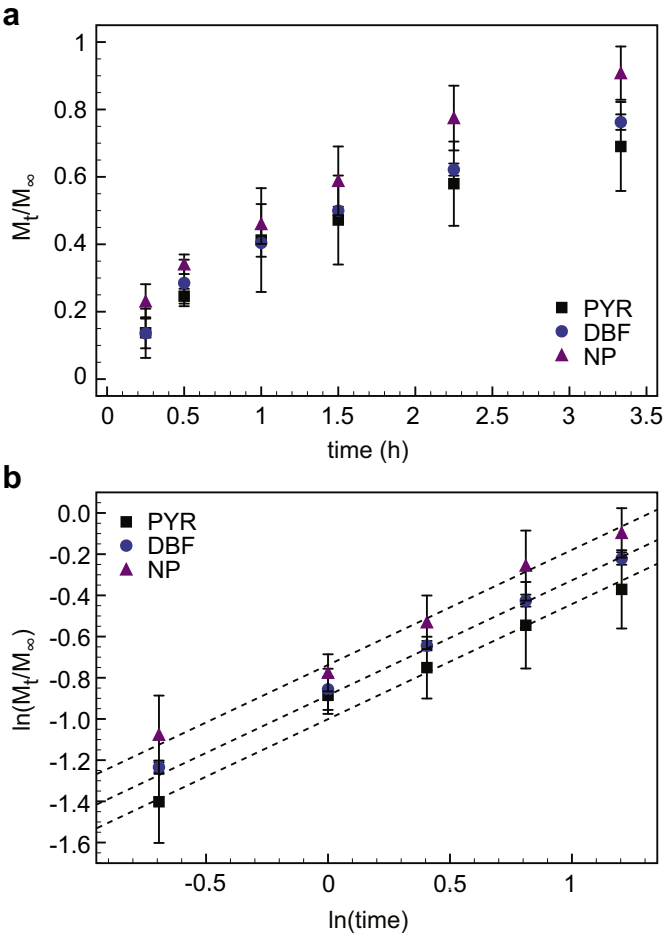

Fig. 4. a. Release of a model drug compound from supramolecular hydrogels prepared with varying physical crosslinking dynamics by employing different second guest functional polymers (PDMAm-G2) for CB[8] complex formation. b. Plot of the release kinetics of a model drug compound demonstrating the dependence of the release rate on the network dynamics of the supramolecular hydrogels. Error bars represent one standard deviation ($n = 3$).

Table 2
Release characteristics of model cargo from supramolecular polymeric hydrogels.[a]

Guest	Ea_d (kJ/mol)[b]	$k_{release}$ (%/h)[c]	n[c]	$k_{erosion}$ (h^{-1})[d]
NP	30 ± 2	48 ± 1.1	0.53 ± 0.03	3.7 ± 0.5
DBF	54 ± 2	42 ± 0.9	0.53 ± 0.01	3.3 ± 0.5
PYR	89 ± 3	38 ± 0.9	0.53 ± 0.04	2.4 ± 0.6

[a] Error values represent one standard deviation.
[b] Determined previously using stopped-flow spectrofluorometric assays [29].
[c] Determined by fitting the release data of Rhodamine-B dye from hydrogels utilizing the Ritger–Peppas equation.
[d] Determined by fitting the erosion data with a single exponential decay function.

developed for covalent hydrogels (*i.e.* where $Ea_d \rightarrow \infty$) using the mesh size determined previously from SAXS measurements [10,45]. The materials investigated in this study, therefore, give an excellent view of the intermediary stages of solute diffusion through a polymeric matrix with a time-dependent mesh size that is visualized in Fig. 6.

Additionally, it is evident from Fig. 7 that a lower energetic barrier to dissociation of the crosslinks (*i.e.* lower Ea_d values) yield faster erosion rates from the polymeric devices than slower crosslink dynamics. The erosion data was fit to a single exponential decay function and the resulting rate constant of erosion ($k_{erosion}$) is shown in Table 2. The more rapid dynamics of the NP guest and the resulting increase in fluid-like behavior (as evidenced by the rheological characterization shown above), therefore, give rise to an increased release constant, while simultaneously leading to an increased erosion rate.

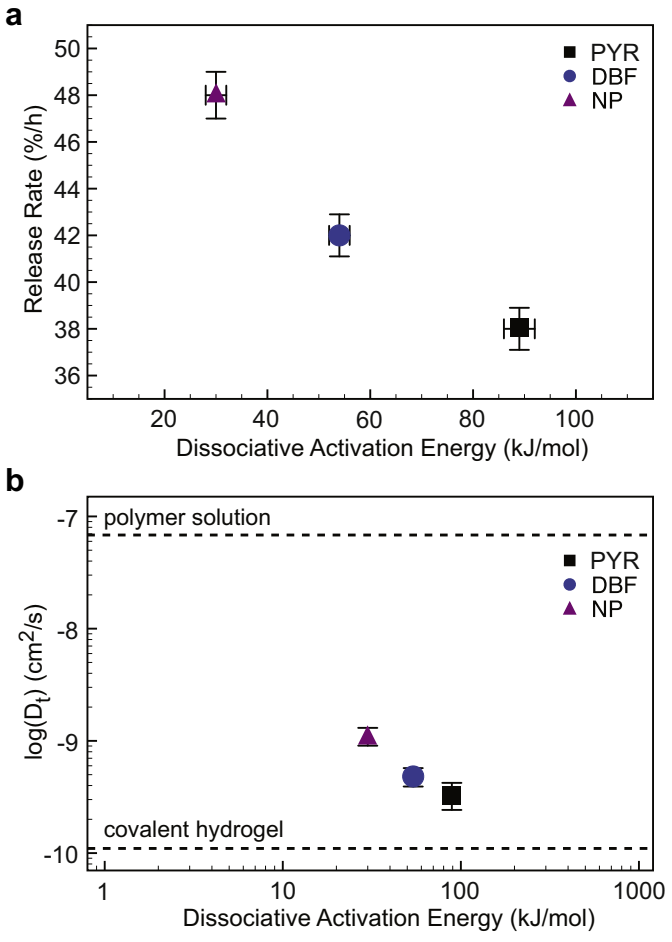

Fig. 5. a. Release rate of a model drug compound from supramolecular hydrogels plotted against the dissociative activation energy of the dynamic crosslinks. b. Plot of the diffusion of the model drug compound through the physically crosslinked hydrogels demonstrating the limits of diffusion through hydrogels with no crosslinking (*i.e.* polymer solution where $Ea_d \rightarrow 0$) and covalent crosslinking (*i.e.* $Ea_d \rightarrow \infty$). Error bars represent one standard deviation ($n = 3$).

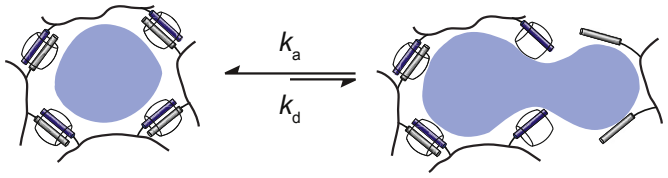

Fig. 6. Schematic representation of the impact of the lifetime of the dynamic physical crosslinks on the time-dependent mesh size of the hydrogels.

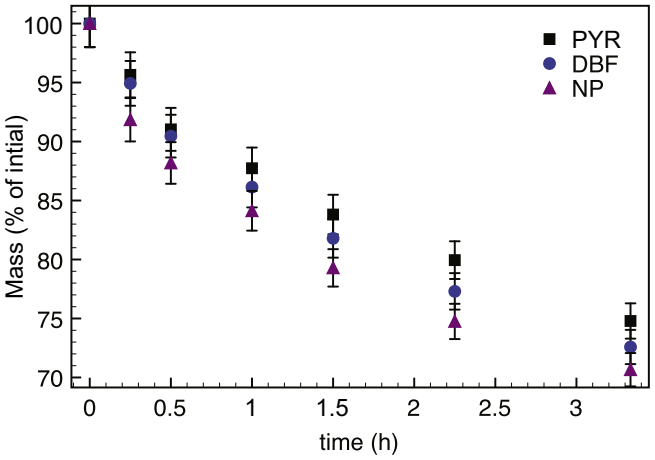

Fig. 7. Plot of the erosion of polymer from the hydrogel demonstrating that slower kinetics in dynamically crosslinked hydrogels leads to slower erosion.

4. Conclusion

A series of physically crosslinked hydrogels have been prepared utilizing host-guest binding interactions of cucurbit[8]uril. These hydrogels have identical strength (plateau modulus), concentration and structure, yet exhibit varying network dynamics on account of the use of different guests for supramolecular crosslinking. The release characteristics of molecular cargo from these hydrogels were investigated and it was quantitatively determined for the first time that the release rate constant was directly correlated with the dynamics of the physical interactions responsible for crosslinking. Moreover, diffusion coefficients for the model drug through the hydrogel matrix highlight that these systems do indeed exhibit a time-dependent mesh size that is bounded by the limiting cases of no crosslinking (*i.e.* $Ea_d \rightarrow 0$) and covalent crosslinking (*i.e.* $Ea_d \rightarrow \infty$). Crosslink dynamics, therefore, play an indispensable role in determining the release mechanism of therapeutic cargo from a hydrogel, demonstrating the importance of understanding the fundamental molecular processes responsible for crosslinking when designing such hydrogel-based drug-delivery systems. Furthermore, this study provides incentive to investigate the impact of crosslink dynamics on diffusion in other areas of science, one particularly important example being diffusion through the natural extracellular matrix (ECM) of various biological tissues.

Acknowledgments

E.A.A. thanks Schlumberger, R.A.F. thanks the Cambridge Commonwealth European and International Trust, and M.J.R.

thanks the University of Cambridge Chemical Biology and Molecular Medicine program for financial support. This work was also supported in part by an ERC Starting Investigator Grant (ASPiRe, 240629) and a Next Generation Fellowship provided by the Walters-Kundert Foundation.

References

[1] Lutolf MP. Spotlight on hydrogels. Nat Mater 2009;8:451–3.
[2] Appel EA, del Barrio J, Loh XJ, Scherman OA. Supramolecular polymeric hydrogels. Chem Soc Rev 2012;41:6195–214.
[3] Seiffert S, Sprakel J. Physical chemistry of supramolecular polymer networks. Chem Soc Rev 2012;41:909–30.
[4] Hoffman AS. Hydrogels for biomedical applications. Adv Drug Deliv Rev 2002;54:3–12.
[5] Sangeetha NM, Maitra U. Supramolecular gels: functions and uses. Chem Soc Rev 2005;34:821–36.
[6] Yu L, Ding J. Injectable hydrogels as unique biomedical materials. Chem Soc Rev 2008;37:1473–81.
[7] Baker RW, Lonsdale HK. Controlled release: mechanisms and rates. New York, NY: Plenum Press; 1974.
[8] Roseman TJ, Cardarelli NF. Monolithic polymer devicesvol. 2. Boca Raton: CRC Press; 1980.
[9] Peppas NA. Mathematical models for controlled release kineticsvol. 2. Boca Raton: CRC Press; 1984.
[10] Crank J. The mathematics of diffusion. Oxford: Clarendon Press; 1975.
[11] Ritger PL, Peppas NA. A simple equation for description of solute release i: fickian and non-fickian release from non-swellable devices in the form of slabs, spheres, cylinders or discs. J Control. Release 1987;5:23–36.
[12] Ritger PL, Peppas NA. A simple equation for description of solute release ii: fickian and anomalous release from swellable devices. J Control Release 1987;5:37–42.
[13] Peppas NA, Sahlin JJ. A simple equation for the description of solute release iii: coupling of diffusion and relaxation. Int J Pharm 1989;57:169–72.
[14] Brannon-Peppas L, Peppas NA. Solute and penetrant diffusion in swellable polymers ix: the mechanisms of drug release from pH-sensitive swelling-controlled systems. J Control Release 1989;8:267–74.
[15] Klier J, Peppas NA. Solute and penetrant diffusion in swellable polymers viii: influence of the swelling interface number on solute concentration profiles and release. J Control Release 1988;7:61–8.
[16] Qiu Y, Park K. Environment-sensitive hydrogels for drug delivery. Adv Drug Deliv Rev 2001;53:321–39.
[17] Peppas NA, Khare AR. Preparation, structure and diffusional behavior of hydrogels in controlled release. Adv Drug Deliv Rev 1993;11:1–35.
[18] Li J, Loh XJ. Cyclodextrin-based supramolecular architectures: synthesis, structures, and applications for drug and gene delivery. Adv Drug Deliv Rev 2008;60:1000–17.
[19] Jeong B, Bae YH, Lee DS, Kim SW. Biodegradable block copolymers as injectable drug-delivery systems. Nature 1997;388:860–2.
[20] Aulisa L, Dong H, Hartgerink JD. Self-assembly of multidomain peptides: sequence variation allows control over cross-linking and viscoelasticity. Biomacromolecules 2009;10:2694–8.
[21] Wojtecki RJ, Meador MA, Rowan SJ. Using the dynamic bond to access macroscopically responsive structurally dynamic polymers. Nat Mater 2010;10:14–27.
[22] Estroff LA, Hamilton AD. Water gelation by small organic molecules. Chem Rev 2004;104:1201–17.
[23] Guvendiren M, Lu HD, Burdick JA. Shear-thinning injectable hydrogels. Soft Matter 2012;8:260–72.
[24] Huynh CT, Nguyen MK, Lee DS. Injectable block copolymers hydrogels: achievements and future challenges for medical applications. Macromolecules 2011;44:6629–36.
[25] Haines-Butterick L, Rajagopal K, Branco M, Salick D, Rughani R, Pilarz M, et al. Controlling hydrogelation kinetics by peptide design for three-dimensional encapsulation and injectable delivery of cells. Proc Natl Acad Sci 2007;104:7791–6.
[26] Chiu YL, Chen SC, Su CJ, Hsiao CW, Chen YM, Chen HL, et al. ph-triggered injectable hydrogels prepared from aqueous *n*-palmitoyl chitosan: *in vitro* characteristics and *in vivo* biocompatibility. Biomaterials 2009;30:4877–88.
[27] Yount WC, Loveless DM, Craig SL. Strong means slow: dynamic contributions to the bulk mechanical properties of supramolecular networks. Angew Chem Int Ed 2005;44:2746–8.
[28] Yount WC, Loveless DM, Craig SL. Small-molecule dynamics and mechanisms underlying the macroscopic mechanical properties of coordinatively cross-linked polymer networks. J Am Chem Soc 2005;127:14488–96.
[29] Appel EA, Forster RA, Koutsioubas A, Toprakcioglu C, Scherman OA. Activation energies control macroscopic properties of physically crosslinked materials. Angew Chem Int Ed 2014. http://dx.doi.org/10.1002/anie.201403192.
[30] Appel EA, Biedermann F, Rauwald U, Jones ST, Zayed JM, Scherman OA. Supramolecular cross-linked networks *via* host–guest complexation with cucurbit[8]uril. J Am Chem Soc 2010;132:14251–60.
[31] Appel EA, Loh XJ, Jones ST, Biedermann F, Dreiss CA, Scherman OA. High-water-content hydrogels from renewable resources through host-guest interactions. J Am Chem Soc 2012;134:11767–73.
[32] Appel EA, Loh XJ, Jones ST, Dreiss CA, Scherman OA. Sustained release of proteins from high water content supramolecular hydrogels. Biomaterials 2012;33:4646–52.
[33] McKee JR, Appel EA, Seitsonen J, Kontturi E, Scherman OA, Ikkala O. Healable, stable and stiff hydrogels: combining conflicting properties using dynamic and selective three-component recognition with reinforcing cellulose nanorods. Adv Funct Mater 2014;24:2706–13.
[34] Zhao N, Liu L, Biedermann F, Scherman OA. Binding studies on CB[6] with a series of 1-alkyl-3-methylimidazolium ionic liquids in an aqueous system. Chem Asian J 2010;5:530–7.
[35] Marquez C, Hudgins RR, Nau WM. Mechanism of host-guest complexation by cucurbituril. J Am Chem Soc 2004;126:5806–16.
[36] Lagona J, Mukhopadhyay P, Chakrabarti S, Isaacs L. The cucurbit[*n*]uril family. Angew Chem Int Ed 2005;44:4844–70.
[37] Liu S, Ruspic C, Mukhopadhyay P, Chakrabarti S, Zavalij PY, Isaacs L. The cucurbit[*n*]uril family: prime components for self-sorting systems. J Am Chem Soc 2005;127:15959–67.
[38] Kim J, Jung IS, Kim SY, Lee E, Kang JK, Sakamoto S, et al. New cucurbituril homologues: synthesis, isolation, characterization and x-ray crystal structures of cucurbit[*n*]uril ($n = 5$, 7 and 8). J Am Chem Soc 2000;122:540–1.
[39] Rauwald U, Biedermann F, Deroo S, Robinson CV, Scherman OA. Correlating solution binding and ESI-MS stabilities by incorporating solvation effects in a confined cucurbit[8]uril system. J Phys Chem B 2010;114:8606–15.
[40] Appel EA, Dyson J, del Barrio J, Walsh Z, Scherman OA. Folding of single polymer chains in water through host-guest interactions. Angew Chem Int Ed 2012;51:4185–9.
[41] Skey J, O'Reilly RK. Facile one pot synthesis of a range of reversible addition–fragmentation chain transfer (RAFT) agents. Chem Commun 2008;35:4183–5.
[42] Biedermann F, Appel EA, del Barrio J, Gruendling T, Barner-Kowollik C, Scherman OA. Postpolymerization modification of hydroxyl-functionalized polymers with isocyanates. Macromolecules 2011;44:4828–35.
[43] Tarcha Peter J, editor. Polymers for controlled drug delivery. Boca Raton: CRC Press; 1991.
[44] Holyst R, Bielejewska A, Szymanski J, Wilk A, Patkowski A, Gapinski J, et al. Scaling form of viscosity at all length-scales in poly(ethylene glycol) solutions studied by fluorescence correlation spectroscopy and capillary electrophoresis. Phys Chem Chem Phys 2009;11:9025–32.
[45] Lustig SR, Peppas NA. Solute diffusion in swollen membranes ix. scaling laws for solute diffusion in gels. J Appl Polym Sci 1988;36:735–47.